Plexcitonic crystals: a tunable platform for light-matter interactions

Ertugrul Karademir,[1] Sinan Balci,[2] Coskun Kocabas,[1] and Atilla Aydinli[1,*]

[1]*Department of Physics, Bilkent University, 06800 Ankara, Turkey*
[2]*Department of Astronautical Engineering, University of Turkish Aeronautical Association, 06790 Ankara, Turkey*
[*]*aydinli@fen.bilkent.edu.tr*

Abstract: Coupled states of surface plasmon polaritons (SPPs) and excitons are collectively called plexcitons [Nano Lett. **8**, 3481 (2008)]. Plexcitonics is an emerging field of research aiming to control light-matter interaction at the nanometer length scale using coupled pairs of surface-plasmons and excitons. Ability to control the interaction between localized excitons and propagating surface-plasmons is important for realization of new photonic devices. In this letter, we report plexcitonic crystals that yield direction-dependent plasmon-exciton coupling. We have fabricated one- and two-dimensional plexcitonic crystals on periodically corrugated silver surfaces, which are loaded with J-aggregate complexes. We show that plasmon-exciton coupling is blocked for some crystal directions when exciton energy falls inside the plasmonic band gap of the periodically corrugated metallic surface.

OCIS codes: (240.6680) Surface plasmons; (230.5298) Photonic crystals; (230.4170) Multilayers; (160.5293) Photonic bandgap materials.

References and links

1. J. P. Reithmaier, G. Sęk, A. Löffler, C. Hofmann, S. Kuhn, S. Reitzenstein, L. V. Keldysh, V. D. Kulakovskii, T. L. Reinecke, and A. Forchel, "Strong coupling in a single quantum dot-semiconductor microcavity system," Nature **432**(7014), 197–200 (2004).
2. T. Bagci, A. Simonsen, S. Schmid, L. G. Villanueva, E. Zeuthen, J. Appel, J. M. Taylor, A. Sørensen, K. Usami, A. Schliesser, and E. S. Polzik, "Optical detection of radio waves through a nanomechanical transducer," Nature **507**(7490), 81–85 (2014).
3. A. Wallraff, D. I. Schuster, A. Blais, L. Frunzio, R.-S. Huang, J. Majer, S. Kumar, S. M. Girvin, and R. J. Schoelkopf, "Strong coupling of a single photon to a superconducting qubit using circuit quantum electrodynamics," Nature **431**(7005), 162–167 (2004).
4. C. Bonnand, J. Bellessa, and J. C. Plenet, "Properties of surface plasmons strongly coupled to excitons in an organic semiconductor near a metallic surface," Phys. Rev. B **73**(24), 245330 (2006).
5. T. Schwartz, J. A. Hutchison, C. Genet, and T. W. Ebbesen, "Reversible switching of ultrastrong light-molecule coupling," Phys. Rev. Lett. **106**(19), 196405 (2011).
6. A. Alù and N. Engheta, "Input impedance, nanocircuit loading, and radiation tuning of optical nanoantennas," Phys. Rev. Lett. **101**(4), 043901 (2008).
7. A. Alù and N. Engheta, "Tuning the scattering response of optical nanoantennas with nanocircuit loads," Nat. Photonics **2**(5), 307–310 (2008).
8. Y. Cui, J. Zhou, V. A. Tamma, and W. Park, "Dynamic tuning and symmetry lowering of Fano resonance in plasmonic nanostructure," ACS Nano **6**(3), 2385–2393 (2012).
9. S. Balci, C. Kocabas, S. Ates, E. Karademir, O. Salihoglu, and A. Aydinli, "Tuning surface plasmon-exciton coupling via thickness dependent plasmon damping," Phys. Rev. B **86**(23), 235402 (2012).
10. N. T. Fofang, T.-H. Park, O. Neumann, N. A. Mirin, P. Nordlander, and N. J. Halas, "Plexcitonic nanoparticles: plasmon-exciton coupling in nanoshell-J-aggregate complexes," Nano Lett. **8**(10), 3481–3487 (2008).
11. R. Esteban, A. G. Borisov, P. Nordlander, and J. Aizpurua, "Bridging quantum and classical plasmonics with a quantum-corrected model," Nat. Commun. **3**, 825 (2012).
12. J. Bellessa, C. Bonnand, J. C. Plenet, and J. Mugnier, "Strong coupling between surface plasmons and excitons in an organic semiconductor," Phys. Rev. Lett. **93**(3), 036404 (2004).

#211601 - $15.00 USD Received 7 May 2014; revised 19 Jul 2014; accepted 15 Aug 2014; published 2 Sep 2014

13. Y. Cao, Z. Wei, C. Wu, H. Li, H. Chen, and K. Cai, "Collimation effect inside complete bandgap of electromagnetic surface resonance states on a metal plate perforated with a triangular array of air holes," Opt. Express **20**(23), 25520–25529 (2012).
14. P. A. Kossyrev, A. Yin, S. G. Cloutier, D. A. Cardimona, D. Huang, P. M. Alsing, and J. M. Xu, "Electric field tuning of plasmonic response of nanodot array in liquid crystal matrix," Nano Lett. **5**(10), 1978–1981 (2005).
15. J. R. Tischler, M. Scott Bradley, Q. Zhang, T. Atay, A. Nurmikko, and V. Bulović, "Solid state cavity QED: Strong coupling in organic thin films," Coupled States Excit. Photons Plasmons Org. Struct. **8**, 94–113 (2007).
16. E. D. Palik, *Handbook of Optical Constants of Solids* (Academic, 1991).
17. W. L. Barnes, T. W. Preist, S. C. Kitson, J. R. Sambles, N. P. K. Cotter, and D. J. Nash, "Photonic gaps in the dispersion of surface plasmons on gratings," Phys. Rev. B Condens. Matter **51**(16), 11164–11167 (1995).
18. S. Balci, C. Kocabas, and A. Aydinli, "Critical coupling in plasmonic resonator arrays," Opt. Lett. **36**(15), 2770–2772 (2011).
19. M. A. Armstrong, I. Géerard, and D. D. Joseph, *Groups and Symmetry* (Springer, 1988), Chap. 24.
20. S. C. Kitson, W. L. Barnes, and J. R. Sambles, "Full photonic band gap for surface modes in the visible," Phys. Rev. Lett. **77**(13), 2670–2673 (1996).
21. T. Okamoto and S. Kawata, "Dispersion relation and radiation properties of plasmonic crystals with triangular lattices," Opt. Express **20**(5), 5168–5177 (2012).
22. F. H'Dhili, T. Okamoto, J. Simonen, and S. Kawata, "Improving the emission efficiency of periodic plasmonic structures for lasing applications," Opt. Commun. **284**(2), 561–566 (2011).
23. H. Frederich, F. Wen, J. Laverdant, L. Coolen, C. Schwob, and A. Maître, "Isotropic broadband absorption by a macroscopic self-organized plasmonic crystal," Opt. Express **19**(24), 24424–24433 (2011).
24. D. Kim, "Effect of the azimuthal orientation on the performance of grating-coupled surface-plasmon resonance biosensors," Appl. Opt. **44**(16), 3218–3223 (2005).
25. S. John, "Strong localization of photons in certain disordered dielectric superlattices," Phys. Rev. Lett. **58**(23), 2486–2489 (1987).
26. J. O. Vasseur, P. A. Deymier, B. Chenni, B. Djafari-Rouhani, L. Dobrzynski, and D. Prevost, "Experimental and theoretical evidence for the existence of absolute acoustic band gaps in two-dimensional solid phononic crystals," Phys. Rev. Lett. **86**(14), 3012–3015 (2001).

1. Introduction

When two oscillators with the same energy are weakly coupled, the coupling can be treated as a perturbation which slightly modifies the dynamics of the oscillators. In the strong coupling case, however, two new eigenstates emerge with entirely different dynamics. A universal fingerprint of strong coupling is the anticrossing behavior, which indicates that the eigenvalues of the strongly coupled system cannot be identical. Anticrossing behavior appears in various coupled systems, such as quantum dots in a photonic crystal [1], sound waves coupled to a nanomembrane transducer [2], or coupling of a single microwave photon to a superconducting circuit [3]. Controlling the coupling strength between the pairs is a challenging task requiring the modification of intrinsic nature of the oscillators such as their lifetime [4–9]. Here, we demonstrate a new platform, i.e. plexcitonic crystals, which provide continuous and reversible tuning of the coupling strength between localized excitons and propagating surface plasmons. The method relies on manipulating the reflection map of the propagating surface-plasmons on periodic surfaces. These periodic surfaces introduce a plasmonic band gap in the reflection map. Energetic position of the band gap depends on the propagation direction of surface plasmons in the crystal. Coupled states of SPPs and excitons define a new wave equation leading to plexcitons [10]. Loading the periodic metallic surface with a thin layer of J-aggregate complex forms a new type of crystal that yields directional formation of plexcitons on a single platform. In certain propagation directions, plexcitonic crystals exhibit enhancement and inhibition of plexciton formation dictated by the symmetry of the crystal. These strategies using plexcitonic crystals with various rotational symmetries will be useful for applications in nanophotonics and quantum optics [11–15].

#211601 - $15.00 USD Received 7 May 2014; revised 19 Jul 2014; accepted 15 Aug 2014; published 2 Sep 2014

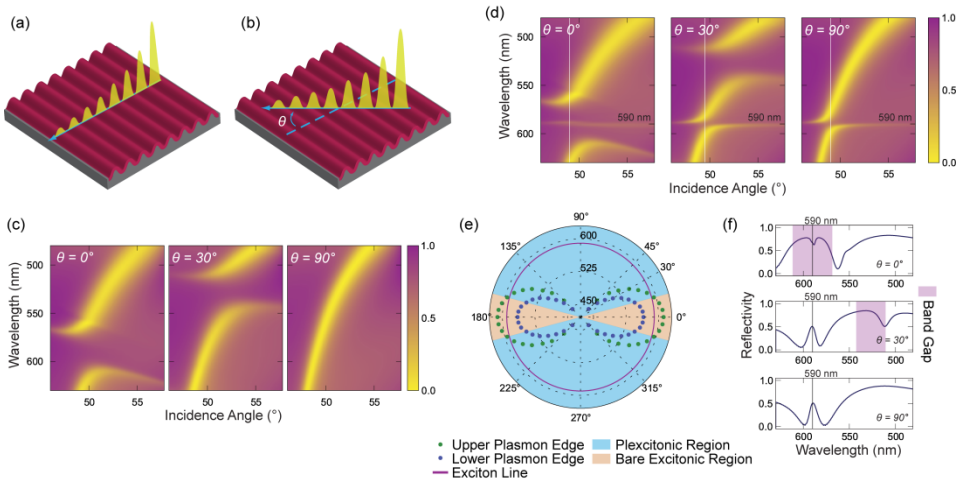

Fig. 1. 1D plexcitonic crystal with grating pitch of 260 nm and depth of 40 nm. (a),(b) are schematic representation of 1D plexitonic crystals and the surface plasmons propagating in directions with the azimuthal angle, θ. (c) Calculated reflection maps of a sinusoidal metallic grating pattern without the excitonic load for three different azimuthal angles. (d) Calculated reflection maps with excitonic load for azimuthal angles of 0°, 30° and 90°, respectively. Its resonance wavelength is at 590 nm. The anticrossing behavior is clearly seen for 30° and 90°. (e) Polar plot showing variation of the upper energy branch (green dots), lower energy branch (blue dots), and exciton energy (purple line) as a function of the propagation direction. (f) Reflection spectra of the plexcitonic crystal at azimuthal angles of 0°, 30° and 90°, and an incidence angle (φ) of 49°.

2. Simulation and experimental methods

For simulations, Finite Difference Time Domain (FDTD) method is employed, which is implemented with a commercial software package from Lumerical Inc. Grating period is set to be either 260 nm or 280 nm. If the crystal is a two dimensional crystal, the pitch is the same for both dimensions. Grating depth is fixed at 40 nm. For each crystal, one unit cell of the grating is confined inside Bloch boundaries in lateral dimensions (x and y). In the stacking direction (z), a SiO_2 substrate coated with a 40 nm Ag film is used and in this direction perfectly matching layers (PML) are used for boundaries. Optical parameters of both materials are taken from Palik [16]. For each incidence angle, reflection maps are recorded by sending white light from the substrate to the silver film, then collecting the reflection by a power monitor. Results are then corrected for the momenta of different wavelengths of light at each incidence angle. Azimuthal angle is defined by the rotation of the incidence plane of the source (y = 0 plane being $\theta = 0°$) of the light source whereas incidence angle is defined by the angle between the propagation vector of the source and z + axis, polarization angle is adjusted so that the electric field is in the plane of incidence. In order to introduce the J-aggregate film into the calculations, we have used a Lorentz absorber model with base permittivity matching that of the PVA film ($\varepsilon = 2.22$, $n = 1.49$). Line-width of the oscillator is set 8.1×10^{12} rad/s with resonance frequency of 3.19×10^{15} rad/s ($\lambda = 590$ nm). Oscillator strength is tuned to match the splitting that is recorded in the experiments. We have set 14 mesh points per effective wavelength and added a further refinement to set the maximum mesh step in every direction as 5 nm. Convergence tests showed that further refinement does not change the results but costs additional computation time.

Experiments have been done with a variable angle ellipsometer that can control the wavelength of the incidence light within 0.1 nm variation and the incidence angle within 0.01°. Samples are mounted on a BK7 half sphere with index matching fluid that has identical optical parameters as BK7 glass. In order to change the azimuthal orientation, we simply

#211601 - $15.00 USD Received 7 May 2014; revised 19 Jul 2014; accepted 15 Aug 2014; published 2 Sep 2014

rotated the half sphere. For each wavelength and incidence angle, we have recorded the reflectivity of the sample from the prism side.

Samples have been prepared with standard holographic lithography. Each sample is coated with Barli II anti reflection coating (ARC) from AZ Chemicals that reduces the reflection from the substrate. On top of this layer AZ 5214E photoresist (PR) from AZ Chemicals is coated. For the exposure, the collimated light from Kimmon He-Cd laser with 21 mW output is focused with a fused silica lens. Just beyond the focal point, airy disk is spatially filtered through a pinhole of 10 μm diameter. Half of the expanded disk is incident upon a Lloyd mirror, which is at right angle with respect to the sample; the other half of the light directly reaches the sample. Hence an interference pattern with tunable periodicity is obtained.

One dimensional crystal samples have been obtained with single exposure, whereas two dimensional crystals are obtained with two exposures, where the second exposure is applied after rotating the sample. Rotation angle of the second exposure is determined by the intended symmetry of the crystal. Square lattice is obtained by 90° rotation of the sample with respect to the first exposure, hexagonal crystal is obtained by 60° rotation. In all exposures, pitch of the grating is set to yield either 260 nm or 280 nm. Exposure time determines the depth of the grating. Resulting grating depth is characterized with an atomic force microscope.

TDBC (5,5′, 6,6’-tetrachloro-di-(4-sulfobutyl) benzimidazole-carbocyanine) dye is used as J-aggregate, which has its absorption peak at 590 nm wavelength. TDBC is dissolved in poly vinyl alcohol (PVA) polymer, which is water soluble and suitable for proper thin film fabrication of aggregated TDBC dye. Dye embedded polymer layer is then spin coated on the silver plated sample. Concentration of TDBC is set 2 mM in 0.75% PVA.

3. One dimensional plexcitonic crystals

Figures 1(a) and 1(b) show a schematic representation of the one-dimensional plexcitonic crystals and surface plasmons propagating in two separate directions. The plexcitonic crystal contains a hybrid metal-organic surface structure of one-dimensional grating uniformly coated within a polymer thin film containing J-aggregates. The azimuthal angle (θ) defines the propagation direction of SPPs. The calculated reflection maps of surface plasmons for azimuthal angles of 0°, 30°, and 90° are shown in Fig. 1(c). When SPPs propagate perpendicular to the grating grooves ($\theta = 0°$), the centre of the plasmonic band gap is located at 590 nm, however, in the parallel direction ($\theta = 90°$), SPPs experience a flat metal that does not exhibit a plasmonic band gap. For intermediate propagation directions, the location of the band gap varies continuously. The plasmonic band gap occurs when the wave-vector of SPP (k_{SPP}) intersects with the Brillouin zone boundary, $k_{SPP} = \frac{\pi}{\Lambda \cos(\theta)}$, where Λ is the period of the metallic surface and θ is the azimuthal angle.

#211601 - $15.00 USD Received 7 May 2014; revised 19 Jul 2014; accepted 15 Aug 2014; published 2 Sep 2014

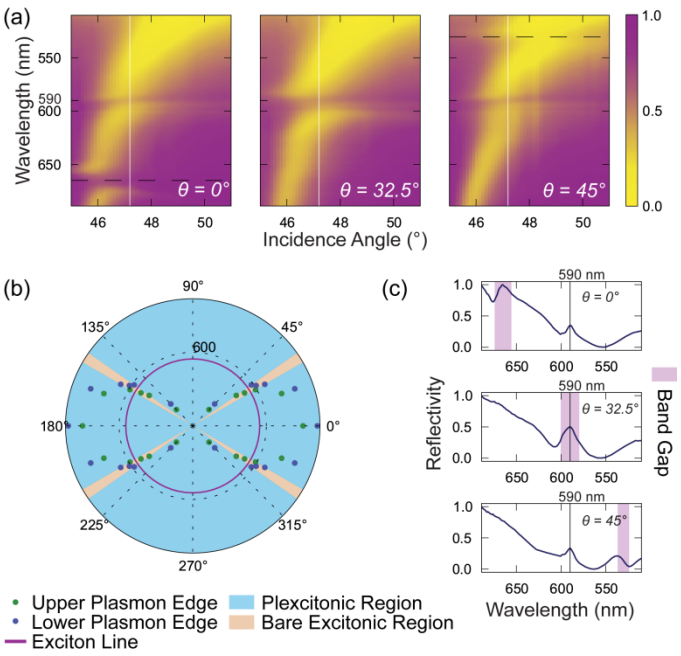

Fig. 2. Experimental realization of 1D plexcitonic crystal with 280 nm pitch with sinus profile. Grating depth is 22 nm ± 1 nm. (a) shows experimental reflection maps, confirming the formation of the plexcitons. Anti-crossing behavior (indicated with solid black line) in the reflection map disappears once the absorption line of TDBC dye is introduced inside the band gap of the plasmonic crystal at 32.5° azimuth. (b) shows directional dependence of plexcitonic and bare excitonic regions. Exciton line intersects the band gap separation at 32.5° azimuth angle. SPP-exciton interaction is significantly weak between 30° and 35° azimuth. In (c), this effect is more pronounced. Band gap separation shifts from around 630 nm to 530 nm. At 32.5° azimuth angle, TDBC absorption line is totally inside the band gap.

When the exciton energy lies in the plasmonic band gap, lack of plasmonic states inhibits plexciton formation. Controlling the propagation direction by simply rotating the sample in the Kretschmann configuration yields the unprecedented ability to tune the plasmon-exciton coupling. Figure 1(d) shows the reflection maps of the plexcitonic crystal for different propagation directions. In contrast with the planar surface where plexciton formation is omnidirectional, there is no plexciton formation at $\theta = 0°$ since the exciton resonance falls inside the plasmonic band gap. The state in the band gap [Fig. 1(d)] is due to the absorption of the bare excitons. As we rotate the sample or vary the propagation direction of SPPs, the position of the band gap shifts to longer wavelengths and plasmon-exciton coupling emerges with a clear anticrossing behavior. The resulting energy gap is characterized by the Rabi frequency, $\hbar\Omega_R = \sqrt{4V^2 - (\gamma_p - \gamma_e)^2}$. Here, Rabi frequency ($\Omega_R$) of SPP-exciton pair depends on the intrinsic properties of excitons and plasmons (the decay rate of the excitons, γ_e and plasmon damping, γ_p) and the interaction strength, $V = g\hbar = \vec{\mu}\cdot\vec{E}$, where μ is the dipole moment of the J-aggregates E is the electric field of the surface-plasmons, and g is the rate of energy transfer. Since the amplitude of the electric field is directly related to the number of plasmonic states at a given energy, exciton-plasmon coupling can be controlled by tuning the position of the plasmonic band gap with respect to the exciton resonance. Polar plot in Fig. 1(e) shows the angular dependence of the upper and lower edges of the plasmonic band gap and the energy of the excitons (590 nm). There are two distinct regions; (1) a plexcitonic region where excitons are coupled with surface plasmons and (2) bare exciton region where exciton energy lies in the plasmonic band gap. Bare exciton region spans an angular range of

#211601 - $15.00 USD Received 7 May 2014; revised 19 Jul 2014; accepted 15 Aug 2014; published 2 Sep 2014

30°. This range can be adjusted by varying the depth of the grating grooves [17,18]. Deeper grooves results in a wider band gap [17]. The reflection spectra from the 1D plexcitonic crystal are given in Fig. 1(f) for three different propagation directions (0°, 30° and 90°). The shaded area shows the location of the plasmonic band gap.

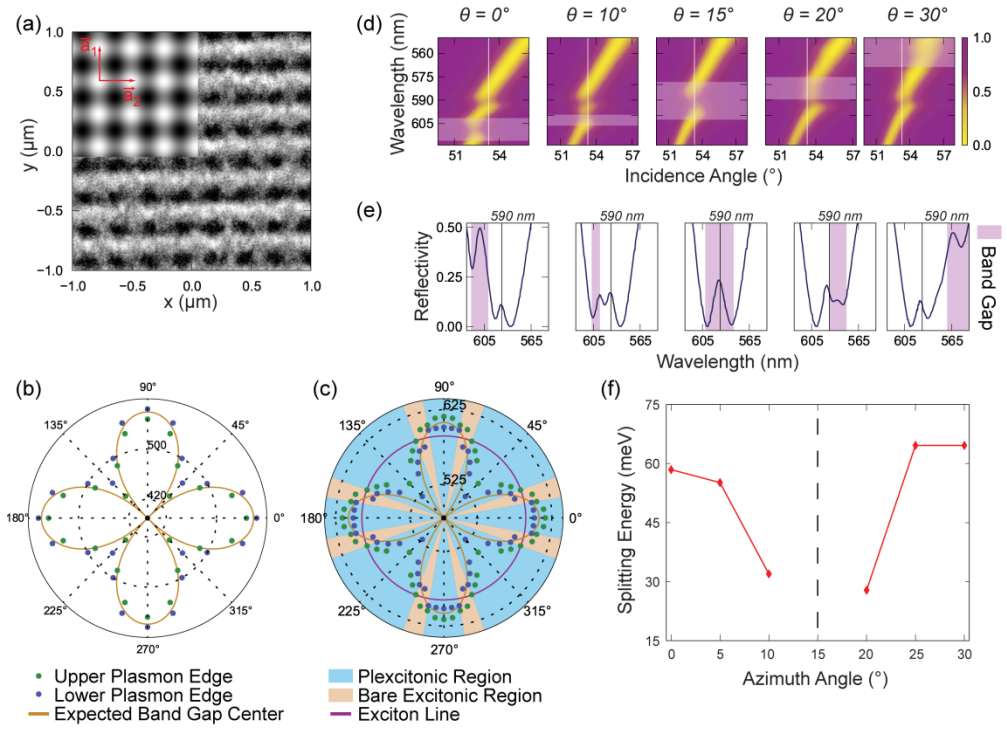

Fig. 3. 2D plexcitonic crystal with square lattice symmetry. Grating pitch in both directions is 280 nm whereas depth of the grating is 41 nm ± 2 nm. In (a) square plexcitonic lattice pattern and a detailed SEM micrograph which confirms the intended geometry; a complete correspondence with the numerical model is presented in the inset together with the unit vectors that build up the crystal. (b) shows the band gap separation as a function of azimuthal angle without the excitonic load. (c) shows plexcitonic and bare excitonic regions after we load the sample with TDBC dye embedded in the PVA matrix. In (c) and (d), the data are repeated with detailed measurements, in accordance with the fourfold rotational symmetry of the crystal. (d) and (e) show the reflection maps and reflection spectra along with the white lines for several different azimuth angles, respectively. At 0° and 30° azimuth angles, a strong anti-crossing behavior is observed. Starting from 10° azimuth angle, coupling of SPPs and excitons weakens resulting in appearance of completely bare excitons at 15° azimuth angle. At 20° azimuth angle, we see the interaction regaining strength and at 30° azimuth interaction strength is completely recovered. This trend can be observed more clearly in (f) where splitting energy as a function of azimuth angle is plotted. At 15° azimuth, anti-crossing cannot be distinguished from the band gap.

Figure 2(a) shows experimental realization of the reflection map of such 1D plexcitonic crystals. At θ = 0° azimuth angle, band gap centre is located at 630 nm. Changing the propagation direction of SPPs from 0° to 45°, the band gap centre shifts to 530 nm. At θ = 32.5°, band gap centre is located at exactly 590 nm and the J-aggregate lies at the centre of the band gap. The polar plot in Fig. 2(b) shows the dependence of the band edge positions on the propagation direction of SPPs. In parallel with the calculations in Fig. 1(e), we observe both plexcitonic and bare excitonic regions in Fig. 2(b). Different from the results shown in Fig. 1(e), bare excitonic regions are narrower in Fig. 2(b), because the grating depth is less than that of the grating depth shown in Fig. 1. It is clear that plexciton formation is inhibited

#211601 - $15.00 USD Received 7 May 2014; revised 19 Jul 2014; accepted 15 Aug 2014; published 2 Sep 2014

inside the plasmonic band gap whereas the plexciton formation can be observed outside the band gap region [Fig. 2(c)].

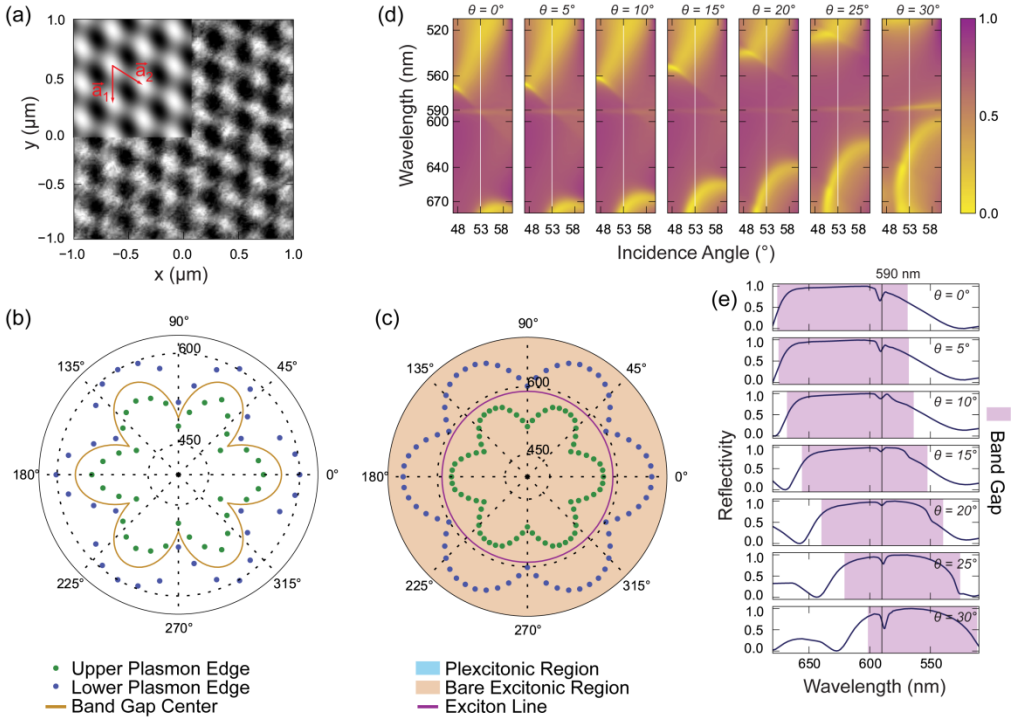

Fig. 4. 2D plexcitonic crystal with triangular lattice symmetry. The 2D plexcitonic crystal is obtained with two super-imposed 1D crystals rotated 60° with respect to each other. The crystal shows a triangular lattice pattern with six-fold rotational invariance. (a) shows the pattern and SEM micrograph of the bare crystal. Unit vectors that build up the crystal are indicated on the diagram. Grating pitch is 280 nm in both directions whereas grating depth is 60 nm ± 2nm. (b) shows experimental results of the directional dependence of the band edges displaying hexagonal pattern without the excitonic load. In (c) simulations show that the exciton line is inside the band gap for all the azimuthal angles. For the simulations, grating pitch is set 280 nm with depth of 80 nm in order to fully enclose the exciton line. (d) and (e) are simulated reflection maps and spectra for particular incidence angles. These are presented for azimuthal angles ranging from 0° to 30°.

4. Two dimensional plexcitonic crystals

Adding another periodic pattern superimposed onto the previous one-dimensional crystal, along a different direction results in a two-dimensional crystal pattern. This structure can be fabricated from a thin layer of photoresist coated on a glass substrate using double exposure in a holographic lithography setup. Thin layer of metal film supports the propagation of SPPs. Propagation direction of SPPs defines the position of the plasmonic band gap position. Resulting crystal pattern depends on the angular orientation of the second grating with respect to the first one and shows a different rotational symmetry for different angular orientations. If the angular orientation is chosen to be 90°, resulting pattern is a square lattice with a four-fold rotational symmetry whereas if this angular orientation is chosen to be 60°, resulting pattern becomes a triangular lattice with six-fold rotational symmetry [19]. Two-dimensional patterns have been previously shown to exhibit omnidirectional band gap [20]. The resulting 2D pattern has been investigated for its resemblance to the electronic structure of an atomic crystal [21], to its role in collimation [13], to the field enhancement observed near the band edges, to the possibility of SPP amplification [22], and for its role in broadband absorption with self organized particles [23]. Implementation of such an approach for plexcitonic

#211601 - $15.00 USD Received 7 May 2014; revised 19 Jul 2014; accepted 15 Aug 2014; published 2 Sep 2014

systems results in interesting physics. Reversible variation of the upper and lower plasmonic band edge energies as a function of propagation direction of SPPs is possible by using a single 2D plexcitonic crystal, thus, is appealing in reversible control of plasmon-exciton interaction. A theoretical survey [24] for a similar scheme only with a ridge grating exists; however, it doesn't involve band edge tuning. To our knowledge, this work is the first investigation of such a system for continuous and reversible tuning of light-matter interaction.

In Fig. 3(a), a numerical simulation of a square lattice plexcitonic crystal where tetragonal arrays of dots project the unit cell, is shown. An SEM picture of the same structure is shown in Fig. 3(a), where the inset delineates the symmetry of the crystal. Four-fold rotational symmetry can be clearly seen in the polar plots of Figs. 3(b) and 3(c) where band edge positions with and without J-aggregate load are, respectively, presented. Varying the propagation direction of SPPs from 0° to 45°, wavelength of the plasmonic band edges in the reflection map exhibits a blue shift. However, for the propagation direction of SPPs greater than 45°, band gap edges show a red shift. When the propagation direction is 90°, the band edge energies are at the same position with the ones obtained at 0° propagation direction. Figure 3(d) shows reflection maps taken at various azimuthal angles. At 0° and 30° azimuth angles, a strong anti-crossing behavior is observed. Starting from 10° azimuth angle, coupling strength of SPPs and excitons weakens resulting in appearance of bare excitons at 15° azimuth angle. At 20° azimuth angle, the Rabi splitting energy increases and hence at 30° azimuth angle, the Rabi energy reaches to its maximum value. Figure 3(e) shows the reflection spectra along the white lines indicated in Fig. 3(d). The shift of the band gap edges is observed in reflection map and exciton energy level inside the band gap can be seen for SPP propagation direction at 15°. As the propagation direction of SPPs on the square lattice plasmonic crystal varies from 0° to 45°, band gap centre in the reflection map exhibits a blue shift of around 500 meV from 540 nm to 430 nm. This range does not coincide with the excitonic line. However, the centre of the plasmonic band gap in the reflection map shifts towards the red after coating the plasmonic crystal with a thin layer of J-aggregate embedded in a polymer film, forming a plexcitonic crystal. This is due to the increase in the effective index of the J-aggregate covered metallic grating. As the propagation direction is varied from 0° to 45°, the band gap centre wavelength shifts from 609 nm to 559 nm. However, excitonic line of J-aggregate lies in the band gap at 15° azimuthal angle. Due to crystal symmetry, this condition repeats itself at approximately at each 90° + 15° and 90°-15° azimuth angles, each with angular span of 10°. In Fig. 3(f), the Rabi splitting energy as a function of propagation direction is presented. Splitting energy is indicative of the coupling strength between the plasmon and the exciton [15]. At 15° azimuth, anti-crossing cannot be distinguished from the band gap separation, however, at 10° and 20° azimuth angles, splitting energy (30 meV) is less than the splitting energy observed at other azimuth angles (60 meV). Figure 4(a) shows the 2D triangular lattice pattern and its SEM image. Six-fold rotational symmetry is clearly seen in Figs. 4(b) and 4(c). Hexagonal arrays of dots are observed. Since the propagation direction of SPPs controls the band edge energy levels in the reflection map, it is possible to shift the band gap centre from 570 nm at 0° azimuth angle to 500 nm at 30° azimuth angle corresponding to a ~300 meV shift of the band gap centre. This lattice has been shown to exhibit a full plasmonic band gap [20]. The depth and the periodicity of the gratings can be adjusted to fully enclose and encircle the excitonic line (80 nm), establishing a fully uncoupled plasmon-exciton interaction landscape, switching from the plexcitonic regime to the bare particle regime. Simulation results of totally bare excitonic region are shown in Figs. 4(d) and 4(e).

5. Conclusion

Crystals are periodic structures that show symmetries under translation and rotation operations. Periodic nature of such structures yields interesting phenomena in photonics and plasmonics. In particular, photonic crystals have been extensively studied for their peculiar

#211601 - $15.00 USD Received 7 May 2014; revised 19 Jul 2014; accepted 15 Aug 2014; published 2 Sep 2014

behavior of blocking the propagation of photons for a band of energies and allowing others [25]. Similar studies have been presented for other wave phenomena such as plasmonic and phononic crystals [26]. In the case of plasmonic crystals, periodic metallic structures have been shown to display forbidden and allowed bands for propagating plasmons in all crystal directions [20]. We have presented a new platform i.e. plexcitonic crystals, that exploits the geometric dependence of SPP propagation to tune the coupling strength of the SPP-exciton pair that leads to formation of plexcitons and demonstrates directional dependence of plexciton formation in 1D and 2D plexcitonic crystals. 2D crystals are fabricated by superposition of two 1D crystals using holographic lithography and consequently exhibit a band gap whose properties can reflect the superposition of the properties of 1D crystals. Plexcitonic crystals show bare excitonic regions where exciton line intersects the edges of the band gap. In 2D case, this is extended further depending on the rotational symmetry of the crystal. These crystals show both a tunable energy range of band gap centre for a broad range of wavelengths in the visible, and allow control of interaction strength of plasmon-exciton pairs.

Acknowledgments

This work has been supported from the Scientific and Technological Research Council of Turkey (TUBITAK) by Grants No. 110T589 and 110T790 . The authors would like to thank S. Gundogdu and S. Saritas for help with sample preparations. EK is grateful to Ergun Karaman for his help in building the omnidirectional Kretschmann configuration setup.